
Learning Invariant Visual Representations for Planning with Joint-Embedding Predictive World Models

Leonardo F. Toso^{*1} Davit Shadunts^{*1} Yunyang Lu^{*1} Nihal Sharma² Donglin Zhan¹
 Nam H. Nguyen² James Anderson¹

Abstract

World models learned from high-dimensional visual observations allow agents to make decisions and plan directly in latent space, avoiding pixel-level reconstruction. However, recent latent predictive architectures (JEPAs), including the DINO world model (DINO-WM), display a degradation in test time robustness due to their sensitivity to “slow features”. These include visual variations such as background changes and distractors that are irrelevant to the task being solved. We address this limitation by augmenting the predictive objective with a bisimulation encoder that enforces control-relevant state equivalence, mapping states with similar transition dynamics to nearby latent states while limiting contributions from slow features. We evaluate our model on a simple navigation task under different test-time background changes and visual distractors. Across all benchmarks, our model consistently improves robustness to slow features while operating in a reduced latent space, up to $10\times$ smaller than that of DINO-WM. Moreover, our model is agnostic to the choice of pretrained visual encoder and maintains robustness when paired with DINOv2, SimDINOv2, and iBOT features.

1. Introduction

Constructing spatial and temporal models of the world to predict future outcomes and guide decisions is a crucial capability of the human brain (Shadmehr & Mussa-Ivaldi, 2012). In machine learning, this is mirrored through world models that are learned from high-dimensional visual observations, enabling efficient prediction, planning, and control by reasoning over learned latent dynamics rather than raw sensory inputs. Planning with such a “compressed” representation of the environment dynamics has become a cornerstone of

contemporary robotics (Ha & Schmidhuber, 2018; Hafner et al., 2020; Zhou et al., 2025), model-based reinforcement learning (RL), and control (Hafner et al., 2019; 2021; Ebert et al., 2018; Thuruthel et al., 2018; Matsuo et al., 2022; Khorrambakht et al., 2025) as it provides data efficiency and generalization across tasks while avoiding online interaction and visual reconstruction (Sobal et al., 2025).

An impactful line of recent work centers on Joint Embedding Predictive Architectures (JEPAs), which eschew reconstruction of raw observations in favor of learning representations by predicting future latent embeddings (Grill et al., 2020; Caron et al., 2021; LeCun, 2022; Assran et al., 2023; Sobal et al., 2025; Balestriero & LeCun, 2025). Building on JEPAs, the DINO world model (DINO-WM) (Zhou et al., 2025) learns a latent predictive dynamic by encoding visual observations through a pretrained DINOv2 feature extractor (Oquab et al., 2023). This yields zero-shot planning, with a pretrained, reward-free world model on entirely new tasks.

Despite their empirical success, JEPAs suffer from a fundamental limitation: they pay too much attention to *slowly changing* and *task-irrelevant features* (LeCun, 2022; Sobal et al., 2022). These slow features refer to aspects of the raw observations that change gradually over time, but are irrelevant for planning, such as background textures, lighting, camera viewpoints, and distractors. In the presence of slow features, the predictive objective in JEPAs can be minimized by encoding *only* such temporally consistent information, yielding degenerate solutions. As a result, world models trained under fixed visual conditions often fail to generalize when the background changes at test time (despite identical underlying object dynamics). This limitation has been discussed in (Sobal et al., 2022) for JEPAs and empirically observed to be true for DINO-WM (Figure 2-(Right)).

Importantly, this limitation *cannot* be fully resolved by larger visual foundation models alone (such as DINOv2 (Oquab et al., 2023), SimDINOv2 (Wu et al., 2025), iBOT (Zhou et al., 2021), masked autoencoders (He et al., 2022), among others) as they also extract control-irrelevant information. Even with invariant perception modules, the learned latent dynamics may still entangle control-relevant states with nuisance visual features, leading to brittle planning

^{*}Equal contribution ¹Department of Electrical Engineering, Columbia University, New York, USA. ²Capital One, USA. Correspondence to: Leonardo F. Toso <leonardo.toso@columbia.edu>.

under visual distribution shifts at test time. Ideally, a world model should encode only those aspects of the state that are relevant for predicting future states, while being invariant to task-irrelevant visual factors.

Question. Can we learn latent world models that retain the joint-embedding predictive strengths while also being robust to the slow features?

We address this question using bisimulation metrics for learning invariant representations on top of pretrained visual feature extractors (i.e., DINOv2, SimDINOv2, iBOT). These metrics define state equivalences based on immediate rewards and transition dynamics, and have been studied as a principled foundation for state abstraction in Markov Decision Processes (MDPs) (Ferns et al., 2004; Castro et al., 2009), transfer learning (Castro & Precup, 2010), and invariant representation learning (Zhang et al., 2021; Kemertas & Aumentado-Armstrong, 2021; Tkachev & Abate, 2011; Shimizu & Tomizuka, 2025). By construction, encoders trained with a bisimulation regularizer discard nuisance features that do not affect control, making it a natural candidate for addressing the slow-feature limitation of JEPAs.

Key Point. DINO-WM (Zhou et al., 2025) displays a substantial degradation in performance on relatively simple navigation tasks (e.g., PointMaze (Fu et al., 2020)) when evaluated under background changes and visual distractors at test time (see Figure 2-(Right)). To address this, we propose a *bisimulation encoder* for visual world models that augments latent dynamics with an on-policy bisimulation objective, enforcing invariance in the learned latent space. The bisimulation encoder is trained jointly with the transition model, enforcing states with similar transition behavior to be mapped to nearby latent embeddings while discarding task-irrelevant visual information (see Figure 1). Importantly, we also show that explicit reward prediction is not fundamental to learning invariant world-model representations, thereby simplifying training.

Contributions. Our main contributions are as follows:

- We propose a bisimulation encoder for visual world models that enforces control-relevant state equivalence while discarding task-irrelevant visual features from pretrained visual feature extractors (e.g., DINOv2, SimDINOv2, iBOT).
- We integrate the bisimulation objective into a latent predictive world model architecture (see Figure 2-(Left)), showing that invariant representations can be learned jointly with the transition model *without* relying on reward prediction.
- We show that our bisimulation encoder yields robust planning performance under several background changes and a moving distractor for a navigation task, with latent embeddings dimensions that are $10\times$ smaller than DINO-WM.
- We validate our model with three different pretrained vi-

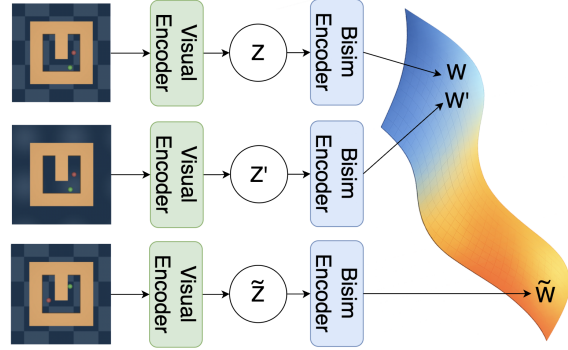


Figure 1. Visually distinct observations that differ only in background (checkerboard and gradient) are first mapped to latent embeddings Z and Z' by a pretrained encoder (initial state in green, goal in red). A bisimulation encoder then projects these into lower-dimensional representations W and W' , which are equivalent under on-policy transition dynamics. In contrast, an observation with different underlying dynamics is mapped to \tilde{W} and separated in the bisimulation space.

sual encoder backbones: DINOv2, SimDINOv2, and iBOT, namely, and show consistent robustness over slow features when compared to DINO-WM (Zhou et al., 2025) both with and without domain randomization (Tobin et al., 2017).

2. Related Work

• **Joint embedding predictive architectures (JEPAs).** Joint embedding predictive architectures learn feature representations by predicting future latent states rather than reconstructing observations (Grill et al., 2020; Caron et al., 2021; LeCun, 2022; Assran et al., 2023; Sobal et al., 2025; Balestriero & LeCun, 2025). Most relevant to our work is DINO-WM (Zhou et al., 2025) that learns latent dynamics directly in the space of pretrained DINOv2 visual features (Oquab et al., 2023), avoiding pixel-level reconstruction. However, latent prediction in DINO-WM remains sensitive to slow, control-irrelevant features. We address this limitation by augmenting the predictive objective with a bisimulation encoder to enforce control-relevant invariances.

• **Bisimulation metrics and invariant representations.** Bisimulation provides a principled way of behavioral equivalence in MDPs by quantifying approximate equivalence through reward discrepancies and mismatches in future state distributions for different states under the same policy (Ferns et al., 2011; Abate, 2013). Most relevant to our work is BS-MPC in (Shimizu & Tomizuka, 2025), which incorporates a bisimulation metric loss for model predictive control (Kouvaritakis & Cannon, 2016; Lenz et al., 2015; Williams et al., 2017). In contrast to (Shimizu & Tomizuka, 2025), we leverage bisimulation metrics to “filter out” control-irrelevant information from a pretrained feature space (e.g., that of DINOv2, SimDINOv2, iBOT). Moreover, we jointly train our prediction model without relying on reward prediction.

• **Model-based control with latent world models.** Model-based RL with world models enable planning by rolling out

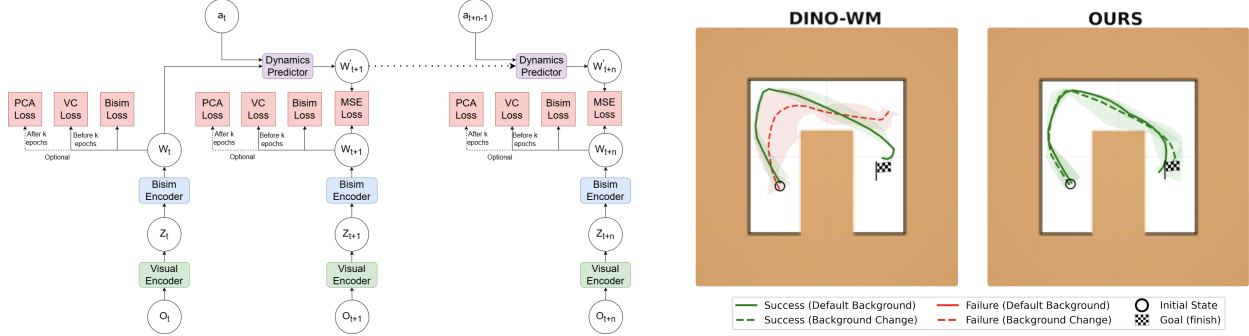


Figure 2. Left. Model architecture and training objectives. Visual observations are encoded using a frozen pretrained visual encoder, followed by a bisimulation encoder that maps features into a low-dimensional, control-relevant latent space. The bisimulation loss is trained jointly with the latent transition model, enforcing invariance to task-irrelevant visual features. **Right.** Rollouts for PointMaze navigation under a background change at test time. For clarity, the background change is not depicted in the figure. See Section 5.3 for details on background changes. While DINO-WM fails to reach the goal due to background change our model succeeds.

learned dynamics in a compact latent space, which has been effective for high-dimensional tasks (Ha & Schmidhuber, 2018; Hafner et al., 2019; 2020). In robotics, latent dynamics models are commonly paired with sampling-based optimizers for action selection, including the cross-entropy method (CEM), which is widely used for planning with learned world models (Rubinstein & Kroese, 2004; Zhou et al., 2025). Our control stack follows this line, we plan with CEM with the learned latent dynamics, and focus on the representation learning side, i.e., how to learn a latent space that is robust to slow features so that planning remains reliable under visual distribution shifts in test time.

3. Preliminaries

We now introduce the notation and preliminaries on JEPAs, bisimulation metrics, and invariant representation learning. Throughout, we consider a vision-based control task given by a partially observable MDP (POMDP) that evolves in discrete time $t \in \{0, 1, 2, \dots\}$. An observation is an RGB image $o_t \in \mathcal{O}$, an action is denoted by $a_t \in \mathcal{A}$, and a trajectory is a sequence $(o_t, a_t, o_{t+1}, a_{t+1}, \dots)$. We denote the data distribution induced by a behavior policy π by \mathcal{D}_π , meaning that $(o_t, a_t, o_{t+1}) \sim \mathcal{D}_\pi$ when rollouts are generated by playing the environment with π . We use $\mathbb{E}_{\mathcal{D}_\pi}[\cdot]$ to denote the expectation with respect to this data distribution.

3.1. Joint-Embedding Predictive Architectures

JEPAs learn a visual encoder $f_\theta : \mathcal{O} \rightarrow \mathbb{R}^{d_z}$ that maps an observation o_t to a latent embedding, i.e., $z_t = f_\theta(o_t) \in \mathbb{R}^{d_z}$, where d_z is the embedding dimension and θ is the vector of encoder parameters. Jointly, a predictor (i.e., latent dynamics model) $\tilde{T}_\phi : \mathbb{R}^{d_z} \times \mathcal{A} \rightarrow \mathbb{R}^{d_z}$ is trained to map the current latent state and action to a predicted next latent state $\hat{z}_{t+1} = \tilde{T}_\phi(z_t, a_t)$, with parameters ϕ .

Since representations are defined up to arbitrary invertible transformations, JEPA training includes a target embedding. The target is denoted by $z_{t+1} = f_\theta(o_{t+1})$. The JEPA objective minimizes the prediction loss between \hat{z}_{t+1} and z_{t+1} ,

$$\mathcal{L}_{\text{pred}}(\theta, \phi) = \mathbb{E}_{\mathcal{D}_\pi} \left[\ell \left(\tilde{T}_\phi(f_\theta(o_t), a_t), f_\theta(o_{t+1}) \right) \right], \quad (1)$$

where $\ell : \mathbb{R}^{d_z} \times \mathbb{R}^{d_z} \rightarrow \mathbb{R}_+$ is the mean squared error.

We emphasize that DINO-WM (Zhou et al., 2025), follow this principle, with the key distinction that the visual encoder parameters θ are fixed and not learned during training. Therefore, observations are first mapped to latent embeddings using a pretrained visual foundation model (e.g., DINOv2 (Oquab et al., 2023)), and a predictive dynamics model is trained on top of that latent space. Here, we also treat the pretrained visual encoder as fixed and train an extra bisimulation encoder jointly with the dynamics on top of it.

Remark 3.1 (Slow Features). We emphasize that JEPAs inadvertently focus on the slow features. In particular, when observations contain static backgrounds or persistent distractors that vary slowly relative to task-relevant dynamics, the prediction loss (1) can be minimized by encoding such features into the latent embedding $z_t = f_\theta(o_t)$, since they induce small temporal differences $\|z_{t+1} - z_t\|$. As a result, slowly varying nuisance information may dominate the predictive objective, leading to latent embeddings that fail to capture the underlying task structure (Sobal et al., 2022) and thus are not generalizable to background changes at test time (see Figure 2-(Right)). This limitation motivates the use of bisimulation. By defining latent distances in terms of on-policy transition behavior, bisimulation induces representations that collapse nuisance visual features while preserving the task-relevant information for planning.

3.2. Bisimulation Metric

Let us now (informally) revisit the definition of on-policy bisimulation metrics from (Castro, 2020). Intuitively, two latent states, in the pretrained visual encoder space, z and z' are “bisimilar” if they induce similar immediate rewards (for optimality equivalence) and similar future state evolution (for dynamics equivalence) under the same actions.

Here, the environment is partially observed and represented through latent embeddings obtained from a visual encoder

(e.g., DINOv2, SimDINOv2, iBOT). The goal is to learn a lower-dimensional representation $w = h_\eta(z) \in \mathbb{R}^{d_w}$, with $d_w \ll d_z$, that preserves control-relevant structure while discarding nuisance visual variation. We formalize state equivalence with the *on-policy* bisimulation metric.

Definition 3.2 (On-Policy Bisimulation Metric (Castro, 2020)). Given a policy π , a reward function $r(z, a)$, and a transition kernel $P_\pi(\cdot | z)$ induced by π , the on-policy bisimulation metric is

$$d_\pi(z, z') = \underbrace{|r_\pi(z) - r_\pi(z')|}_{\text{reward similarity}} + \gamma \underbrace{W_1(P_\pi(\cdot | z), P_\pi(\cdot | z'))}_{\text{dynamics similarity}},$$

where $r_\pi(z) = \mathbb{E}_{a \sim \pi(\cdot | z)}[r(z, a)]$, $\gamma \in (0, 1)$ is a discount factor, and W_1 denotes the 1-Wasserstein distance.

On Dropping the Reward Term. Note that $d_\pi(z, z')$ has two terms: a reward similarity term $|r_\pi(z) - r_\pi(z')|$ and a dynamics similarity term measured via the 1-Wasserstein distance (Givens & Shortt, 1984). The reward term ensures that if two state trajectories are similar, they are not collapsed if they yield different rewards. In particular, such reward discrepancy is crucial when bisimulation is used for policy transfer or value-function approximation (Ferns et al., 2004; Castro et al., 2009; Castro & Precup, 2010). However, for the purpose of learning an invariant representation for JEPAs, we claim that this term is not fundamental. This is because the transition term alone induces a meaningful notion of equivalence: states that exhibit similar evolution under the same action sequences are mapped to nearby representations in the bisimulation latent space (see the illustration in Figure 1)

Moreover, dropping the reward term is well aligned with JEPAs, which are inherently reward-free and focus on predictive consistency in latent space. Incorporating rewards would require task-specific supervision and would break the modularity between representation learning and zero-shot downstream planning. Accordingly, we omit the reward term in our implementation and rely only on approximating the Wasserstein transition similarity to enforce invariance. This design choice is further supported numerically in Section 5, where a reward predictor is included.

3.3. Learning Invariant Representations

Now, we discuss the invariant representation learning problem for our joint-embedding predictive world model. Recall that $z_t = f_\theta(o_t) \in \mathbb{R}^{d_z}$ typically contains both control-relevant information and nuisance features. Our goal is to learn an encoder $w_t = h_\eta(z_t) \in \mathbb{R}^{d_w}$, that limits the contribution of the slow features in the transition dynamics.

To do so, we jointly learn the dynamics in the bisimulation space through $T_\phi : \mathbb{R}^{d_w} \times \mathcal{A} \rightarrow \mathbb{R}^{d_w}$, such that

$\hat{w}_{t+1} = T_\phi(w_t, a_t)$ predicts the next latent state. With the notation set up in Section 3.1, we have the predictive dynamics augmented with the bisimulation encoder, i.e., $T_\phi(h_\eta(f_\theta(o_t)), a_t)$, where again θ is fixed.

To connect invariance to bisimulation, we consider an abstract state space $\mathcal{W} \subseteq \mathbb{R}^{d_w}$ equipped with the metric d_π . We aim to learn h_η and T_ϕ jointly so that the distances in \mathcal{W} approximate an on-policy bisimulation metric, meaning that states that are equivalent for control under rollouts are mapped nearby in such latent space. We do this by optimizing a bisimulation objective that aligns pairwise latent distances with a target quantity that compares on-policy dynamics. Concretely, for a pair of observation, action, and next observation (o_t, a_t, o_{t+1}) and (o'_t, a'_t, o'_{t+1}) drawn from \mathcal{D}_π , we have the latent states

$$\underbrace{z_t = f_\theta(o_t), z'_t = f_\theta(o'_t)}_{\text{Pretrained latents}}, \underbrace{w_t = h_\eta(z_t), w'_t = h_\eta(z'_t)}_{\text{Bisimulation latents}}.$$

The transition dynamics T_ϕ is trained using

$$\mathcal{L}_{\text{dyn}}(\eta, \phi) \triangleq \mathbb{E}_{\mathcal{D}_\pi} [\|h_\eta(f_\theta(o_{t+1})) - T_\phi(h_\eta(f_\theta(o_t)), a_t)\|_2^2],$$

and we note that, in practice, as we do not have \mathcal{D}_π , we compute the empirical mean instead (i.e., MSE).

On the other hand, for invariance, our loss encourages the distance $\|w_t - w'_t\|_2$ to match a control-relevant similarity signal measured by the bisimulation metric. We define the on-policy one-step bisimulation target between states as $\Delta_{\text{bisim}}(\eta, \phi) \triangleq \gamma \|T_\phi(w_t, a_t) - T_\phi(w'_t, a'_t)\|_2$, where it compares the predicted next latent states under the learned dynamics. We fit the bisimulation encoder by minimizing

$$\mathcal{L}_{\text{bisim}}(\eta, \phi) \triangleq \mathbb{E}_{\mathcal{D}_\pi} [(\|w_t - w'_t\|_2 - \Delta_{\text{bisim}}(\eta, \phi))^2].$$

Finally, we define the overall training objective as

$$\mathcal{L}_{\text{jepa-bisim}}(\eta, \phi) \triangleq \mathcal{L}_{\text{dyn}}(\eta, \phi) + \lambda_{\text{bisim}} \mathcal{L}_{\text{bisim}}(\eta, \phi), \quad (2)$$

with $\lambda_{\text{bisim}} > 0$ being the regularization weight.

Minimizing the loss formalizes our goal of learning a compact latent space that preserves on-policy predictive structure for planning while suppressing task-irrelevant visual features. We next describe the architecture, loss instantiation, and planning in the learned bisimulation space.

4. Our World Model

We now describe our architecture for learning invariant world models that builds on pretrained visual features (DINOv2, SimDINOv2, and iBOT) and augments them with a bisimulation encoder to suppress task-irrelevant information. The model learns latent transition dynamics and performs planning via MPC with CEM. An overview of the full pipeline and training objectives is shown in Figure 2-(Left).

4.1. Pretrained Visual Encoders

In our experiments, we consider three self-supervised visual encoders: DINOv2 (Oquab et al., 2023) (with ViT-S/14), SimDINOv2 (Wu et al., 2025) (with ViT-B/16), and iBOT (Zhou et al., 2021) (with ViT-S/16). These are trained on large-scale image datasets using joint embedding or masked prediction objectives and have been shown to produce semantically rich visual features (Jiang et al., 2023).

These visual encoders are *patch-based*, namely, $f_\theta : \mathcal{O} \rightarrow \mathbb{R}^{N_p \times d_z}$, where N_p is the number of patches. Most importantly, they are trained without access to the transition dynamics, actions and/or rewards, and thus capture *generic* visual features rather than control-relevant structure. In particular, they are not tailored for planning and are not fine-tuned to allow for visual shifts in test time. Our goal is to adapt their feature embeddings by learning an additional bisimulation encoder on top of $\{z_t\}_t$ (see Figure 2-(Left)).

When using DINOv2 features, we refer to our model as DINO-Bisim. Similarly, we use SimDINO-Bisim and iBOT-Bisim when paired with SimDINOv2 and iBOT visual feature extractors, respectively.

4.2. Bisimulation Encoder

Given pretrained visual embeddings z_t , we learn a bisimulation encoder $h_\eta : \mathbb{R}^{N_p \times d_z} \rightarrow \mathbb{R}^{N_p \times d_w}$, $w_t = h_\eta(z_t)$, as discussed in Section 3.2. We note that in contrast to (Zhang et al., 2021; Shimizu & Tomizuka, 2025), our bisimulation encoder is designed in patches (we refer the reader to Appendix A.1.3 for details). Such encoder consists of a per-patch residual MLP projection head (Linear-ResMLP-Linear) that maps each DINOv2 patch embedding (or raw image patch) into a $d_w = 32$ dimensional latent, followed by learned spatial positional embeddings and LayerNorm.

This encoder is trained to ensure that distances in the w -space reflect on-policy bisimulation distances, as defined in (2). To this end, we *flatten* the spatial patch features prior to computing the previously defined losses and compare states across different trajectories that are stored in a *replay buffer*, following (Zhang et al., 2021). However, minimizing the bisimulation loss admits degenerate solutions as mapping all states to a single representation trivially minimizes pairwise distances, and we refer to this as the *representation collapse*. To circumvent such collapse, prior work (Bardes et al., 2021; Zhu et al., 2023) has adopted variance-invariance-covariance regularization (VICReg) to guarantee that each latent dimension keeps sufficient variance over batches of states. We refer the reader to (Bardes et al., 2021, Section 4.1) for an excellent overview of the approach. Here, invariance is given by the bisimulation loss.

In our setting, however, the standard VICReg (Bardes et al., 2021) *may be* insufficient. This is because, for the pretrained visual encoders considered in this work (i.e., DI-

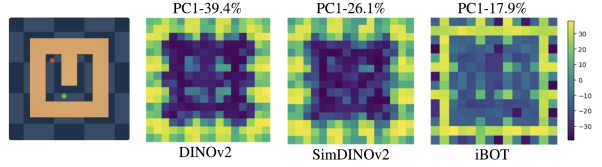


Figure 3. First principal component (PC1) of latent embeddings produced by different visual feature encoders for a PointMaze observation. In all cases, PC1 captures a large percentage of the total variance and predominantly encodes background and layout information rather than control-relevant features, motivating our PCA-based VICReg in the bisimulation encoder.

NOv2, SimDINOv2, and iBOT) a large fraction of the variance is often concentrated in a small number of principal components that correlate with the slow features rather than task-relevant dynamics. Therefore, by imposing a uniform variance across all coordinates may preserve nuisance visual features, preventing the bisimulation encoder from collapsing the task-irrelevant information (see Appendix A.2).

Leveraging this insight, we propose a PCA-based VICReg loss, which adapts VICReg to pretrained visual embeddings by guaranteeing a minimum variance in directions that are not dominated by a large fraction of slow features.

4.3. PCA-based Variance Covariance Regularization

As illustrated in Figure 3, the pretrained visual embeddings from DINOv2, SimDINOv2, and iBOT, allocate a large amount of variance to the first principal component (PC1), which are correlated with task-irrelevant features coming from backgrounds and distractors. If we use the standard VICReg loss with uniform variance across the coordinates of the bisimulation latent space, the optimizer may still preserve such irrelevant directions simply to satisfy the variance threshold, conflicting with the goal of learning a representation invariant to those slow features.

Therefore, we do VICReg in the PCA basis of the current batch. Let $W_c \triangleq [(w_1 - \bar{w})^\top \dots (w_B - \bar{w})^\top]$, be the matrix with centered embeddings in the batch of size B , where \bar{w} is the average. We define the empirical covariance $\Sigma \triangleq \frac{W_c^\top W_c}{B-1}$, and further compute its eigendecomposition as $\Sigma = U\Lambda U^\top$, where $\Lambda = \text{diag}(\lambda_1, \dots, \lambda_{d_w})$. We extract the PCA coordinates $\tilde{w}_b = U^\top(w_b - \bar{w})$, and let \tilde{W}_c be the batch matrix with rows \tilde{w}_b^\top .

To construct the PCA-based VICReg loss, we only enforce the variance floor on the tail PCs, namely indices $i \in \{i_0, \dots, d_w\}$, where i_0 is a cutoff index (e.g., $i_0 = 2$). Let $\kappa_i \triangleq \sigma_{\min} - \sqrt{\lambda_i} + \epsilon$ and write the variance term

$$\mathcal{L}_{\text{pca-var}}(\eta) \triangleq \frac{1}{d_w - i_0 + 1} \sum_{i=i_0}^{d_w} [\max(0, \kappa_i)]^2.$$

where $\epsilon > 0$ is a small constant for numerical stability and σ_{\min} denotes a minimum standard deviation. On the other hand, we regularize cross-covariances as

$$\mathcal{L}_{\text{pca-cov}}(\eta) \triangleq \frac{1}{d_w(d_w - 1)} \sum_{p \neq q} \left(\tilde{\Sigma}_{pq} \right)^2, \quad \tilde{\Sigma} \triangleq \frac{\tilde{W}_c^\top \tilde{W}_c}{B - 1},$$

where $\tilde{\Sigma}_{pq}$ denotes the (p, q) entry of the covariance in PCs coordinates, namely, the covariance matrix $\tilde{\Sigma}$.

Therefore, we combine the two PCA-based terms

$$\mathcal{L}_{\text{pca-vc}}(\eta) \triangleq \alpha_v \mathcal{L}_{\text{pca-var}}(\eta) + \alpha_c \mathcal{L}_{\text{pca-cov}}(\eta),$$

with weights $\alpha_v, \alpha_c > 0$, to the predictive loss (2).

We refer the reader to Appendix A.2 for details on how the PCA-based VICReg loss is implemented and empirical evidence on how it helps the representation collapse while keeping control-relevant features. We emphasize that if the visual encoder does not isolate control-irrelevant features within a dominant principal component, the PCA-based VICReg regularization becomes *optional*. In this case, the bisimulation-based encoder alone can mitigate, though only partially, the influence of task-irrelevant variations in the learned representation.

On the PCA-based VICReg. By not enforcing a minimum variance on the leading PCA components $i < i_0$, the bisimulation encoder can collapse the directions that are dominated by slow features, which concentrate in the top components of the pretrained features. At the same time, enforcing a variance floor on the tail components $i \geq i_0$ prevents $w \equiv \text{constant}$ and ensures that the representation retains sufficient diversity to separate control-relevant states. The covariance loss further yields information to be spread across coordinates.

Implementation. Our bisimulation encoder is initialized with random parameters and is first trained using the standard VICReg objective (Bardes et al., 2021) for a small number of epochs (k) to stabilize representation learning. We then perform a one-time principal component analysis to identify the dominant direction associated with task-irrelevant information. After k (to be set by the practitioner) epochs, we replace the standard VICReg loss with the PCA-based one, which helps to suppresses the additional variance along the identified principal component directions.

4.4. Transition Model

We model latent dynamics using a vision transformer that predicts the next state in the bisimulation latent space. Following DINO-WM (Zhou et al., 2025), the vision transformer architecture (Dosovitskiy, 2020) is suitable for processing the underlying patch-based embeddings. Since the bisimulation latent states are already represented as sequences of patch embeddings, we remove the ViT tokenization layer, yielding a decoder-only transformer.

The transition model takes as input a history of past bisimulation latent states and actions across multiple trajectories,

$\{(w_{j,t-H:t-1}, a_{j,t-H:t-1})\}_{j=1}^{N_{\text{traj}}}$, where H denotes the context length and N_{traj} the number of trajectories, and it predicts the next latent state \hat{w}_t (i.e., in the bisimulation space). Note that the subscript j denotes the trajectory embedding and action at time step t .

To respect temporal causality, a causal attention mask is implemented (as in (Zhou et al., 2025)) ensuring that predictions at time t depend only on past latent states and actions. More precisely, each patch embedding w_t^i attends to the corresponding patch embeddings $\{w_{t-H:t-1}^i\}_{i=1}^{N_p}$ over the context. Predicting all patches jointly yields global spatial structure and temporal dynamics that improves temporal generalization as discussed in (Zhou et al., 2025).

By “filtering out” task-irrelevant visual features, the bisimulation encoder enables the transition model to learn dynamics that are invariant. The learned joint-embedding predictive world model is then used for planning via MPC (Kouvaritakis & Cannon, 2016), with actions selected using the cross-entropy method (CEM).

4.5. Planning

The MPC approach selects the actions whose predicted latent rollouts reach a desired goal observation. That is, given an initial observation o_0 and a goal observation o_g , our model will first compute their latents through the pretrained visual and bisimulation encoders,

$z_0 = f_\theta(o_0)$, $z_g = f_\theta(o_g)$, $w_0 = h_\eta(z_0)$, $w_g = h_\eta(z_g)$. Starting from w_0 , the transition model is used to rollout predicted states under a candidate action sequence $\{a_t\}_{t=0}^{T-1}$, i.e., $\{\hat{w}_{t+1}\}_{t=0}^{T-1} = T_\phi(\hat{w}_t, \{a_t\}_t)$, with $\hat{w}_0 = w_0$. Planning is then cast as minimizing a terminal cost that is the difference between the predicted final latent state and the goal latent state,

$$c(w_T, \{a_t\}_t) = \|\hat{w}_T(\{a_t\}_t) - w_g\|^2. \quad (3)$$

For brevity, we omit the explicit dependence on the action sequence and write $c(w_T) = \|\hat{w}_T - w_g\|^2$.

4.6. A Generalization Bound

Before turning to the experiments, we also provide a theoretical justification for learning bisimulation-based representations on top of JEPA latents. Let us first define the T -step on-policy cost-to-go as follows:

$$J_T^\pi(z) \triangleq \mathbb{E} \left[\sum_{t=0}^{T-1} \gamma^t c(h_\eta(z_t)) \mid z_0 = z \right], \quad z_{t+1} \sim P_\pi(\cdot \mid z_t),$$

where the expectation is taken over trajectories $\{z_t\}_{t=0}^T$ induced by policy π and transition kernel P_π starting from a visual pretrained latent state $z_0 = z$.

Theorem 4.1 (Reward-free planning generalization bound). *Suppose $h_\eta(\cdot)$ ε -approximately preserves the reward-free*

bisimulation metric in the sense that

$$\|h_\eta(z) - h_\eta(z')\|_2 - d_\pi(z, z') \leq \varepsilon, \text{ for any } z, z'.$$

In addition, suppose that $h_\eta(\cdot)$ is uniformly bounded as $\|h_\eta(z)\|_2 \leq H_w$ for all z and thus $\|w_g\|_2 \leq H_w$. Then for any two pretrained visual latent embeddings z, z' ,

$$|J_T^\pi(z) - J_T^\pi(z')| \leq 8H_w T d_\pi(z, z').$$

We defer the proof of this result to Appendix A.8.

We also note that the linear dependence on the horizon T contrasts with the $(1-\gamma^T)/(1-\gamma)$ dependence from (Zhang et al., 2021; Shimizu & Tomizuka, 2025). This difference arises from dropping the reward term in the bisimulation metric: while reward-aware bisimulation enables geometric discounting of cost discrepancies through immediate reward alignment, a reward-free metric propagates the discrepancies through the transition dynamics, yielding a cumulative horizon-dependent bound. In this sense, the T factor can be interpreted as the price paid for enforcing control-relevant invariance without task-specific reward supervision.

Key Takeaway. The above result implies that if two latent states in the pretrained visual encoder space differ only due to nuisance visual variations, such as slow features, then their induced planning behavior remains similar. More concretely, let $z = f_\theta(o)$ embed a PointMaze scene with a checkerboard background, and let $z' = f_\theta(o')$ embed the same scene with a gradient background (see Figure 1), since these visual changes do not affect on-policy transition behavior, the bisimulation distance $d_\pi(z, z')$ is small. Consequently, the difference in the induced planning cost is bounded by $\mathcal{O}(d_\pi(z, z')T)$. Therefore, robustness of planning when starting from w or w' in the bisimulation latent space is governed by their distance in that space.

5. Experiments

We now evaluate our world model. Our experiments assess robustness to slow, task-irrelevant visual features, such as background changes and distractors, and isolate their impact on the planning performance. We compare our model to DINO-WM (Zhou et al., 2025) and domain randomization (DR) (Tobin et al., 2017) for a simple navigation task under different visual conditions, and pretrained visual encoders.

5.1. A Simple Navigation Task

We evaluate our model on a simple navigation task: the MuJoCo PointMaze (Fu et al., 2020). This is commonly used as benchmark for goal-conditioned planning and navigation from visual observations (Fu et al., 2020; Sobal et al., 2025; Zhou et al., 2025; Parthasarathy et al., 2025). Despite its

simplicity, PointMaze provides a controlled setting to assess robustness to background changes and distractors, while keeping the transition dynamics fixed. Further details on the task setup are provided in Appendix A.3.

Although PointMaze is a fairly simple navigation task, we observe that DINO-WM has a substantial drop in the performance under test-time background changes and moving distractors. This highlights that even for a simple task, sensitivity to slow features can negatively impact planning, motivating the need for an invariant latent representation.

Evaluation Metric. We report performance using the success rate (SR), defined as the fraction of successful episodes over 50 independently sampled initial and goal pairs. An episode is considered successful if the agent approximately reaches the goal region within a fixed number of steps.

5.2. Baseline

We compare our model with two baselines: DINO-WM (Zhou et al., 2025) and domain DR (Tobin et al., 2017). Both baselines are evaluated under the same task, planning horizon, and evaluation metric previously described.

DINO-WM. We use the original DINO-WM architecture as proposed in (Zhou et al., 2025). The model operates directly on pretrained DINOv2 patch embeddings with 196 patches, each of dimensionality 384, and learns latent dynamics without explicit invariance regularization. DINO-WM is trained with a batch size of 32.

Domain Randomization (DR). We also train DINO-WM with domain randomization (Tobin et al., 2017). In particular, we randomize the visual appearance of the task for 40% of the training dataset by applying background color changes and gradient-based background modifications, for the PointMaze task. To avoid introducing spurious temporal artifacts, the randomized background is kept consistent across trajectories. We refer the reader to Appendix A.5.

Our model adopts the same number of visual patches (i.e., 196) as DINO-WM, but introduce a bisimulation encoder that maps each patch to a 32-dimensional latent embedding (see Figure 6). This leads to a latent space that is $10\times$ lower-dimensional than the 384-dimensional patch embeddings used by DINO-WM. Our model is trained with a batch size of 20. We refer the reader to Appendix A.1.4 for details on the model hyperparameters.

5.3. Background Changes

We consider different background changes and a moving distractor (see Figure 4) that alter the visual appearance of the scene while preserving the underlying transition dynamics. These changes are applied only at test time, unless otherwise stated, and are designed to isolate the effect of slow features on the planning performance.



Figure 4. The six different scenarios that we use to measure robustness based on PointMaze with checkerboard background. From left to right, these are: **NC**: No Change, **SC**: Slight background Change, **C**: Color gradient background, **LC**: Large Color background Change, **LCG**: Large Color Gradient background change, and **D**: moving Distractors with yellow and magenta dots.

5.4. Results

Table 1 reports the success rate for the PointMaze task under background changes and a moving distractor. Results for PointMaze correspond to models trained for 50 epochs.

Robustness to the background. We note that DINO-WM displays degradation in performance when the visual background is different from the one seen when training (NC). For instance, in the PointMaze task, while DINO-WM achieves 0.8 success rate under NC, its performance drops for SC, 0.72, and it drops even more under aggressive changes, such as LCG, achieving 0.48 success rate.

In contrast, our model consistently achieves high success rates across background changes in PointMaze (around 0.76 success). This highlights that invariance with the bisimulation encoder effectively “filters out” background-dependent features from the latent dynamics, leading to reliable planning despite significant visual changes.

Comparison with DR. Domain randomization performs well when test-time backgrounds resemble combinations of visual changes observed during training (0.82 success rate for NC, SC, and C). However, its performance degrades substantially under an aggressive background change (LCG) that are not covered by the randomized training distribution, i.e., achieving 0.64 success rate.

Moving distractor. Under the moving distractor, DINO-WM again has its performance dropped, indicating that persistent but task-irrelevant motion in the background can also dominate the learned latent dynamics. Our model remains consistent, as the distractor does not affect the transition dynamics and is then suppressed by the bisimulation encoder.

Table 1. Success rate of DINO-Bisim under different scenarios (Figure 4) compared to DINO-WM with and without DR.

| Model | NC | SC | C | LC | LCG | D |
|-------------|------|------|------|------|------|------|
| DINO-WM | 0.80 | 0.72 | 0.60 | 0.56 | 0.48 | 0.78 |
| w/DR | 0.82 | 0.82 | 0.82 | 0.68 | 0.64 | 0.82 |
| Ours | 0.78 | 0.80 | 0.76 | 0.86 | 0.78 | 0.82 |

5.5. On Different Pretrained Visual Encoders

Table 2 reports the success rate achieved by our model when using different pretrained visual encoders. We observe that

training the model *end-to-end* without DINOv2 features results in a clear degradation in performance (e.g., a success rate of 0.26 under LC) compared to training with DINOv2 (0.86 success rate under LC). This behavior is expected, as learning accurate latent transition dynamics relies on sufficiently informative visual representations.

We further evaluate robustness using SimDINOv2 and iBOT features. SimDINOv2 (with ViT-B/16) produces patch embeddings of higher dimensionality than DINOv2 (768 compared to the 384 of DINOv2). As all models are trained with the same number of samples, the larger feature dimensionality may lead to a lower success rate (for example due to overfitting). Nevertheless, performance remains consistent across background changes, indicating that our bisimulation encoder continues to suppress task-irrelevant visual features coming from SimDINOv2 embeddings.

On the other hand, with iBOT features our model achieves strong planning performance (around 0.72 success rate) and robustness comparable to the model with DINOv2, further indicating that the proposed approach generalizes to different pretrained visual encoders.

Table 2. Success rate with different pretrained visual encoder backbones under the different scenarios from Figure 4.

| Model | NC | SC | C | LC | LCG | D |
|---------------|------|------|------|------|------|------|
| No Encoder | 0.68 | 0.44 | 0.70 | 0.26 | 0.36 | 0.64 |
| DINOv2 | 0.78 | 0.8 | 0.76 | 0.86 | 0.78 | 0.82 |
| SimDINOv2 | 0.40 | 0.38 | 0.36 | 0.42 | 0.42 | 0.36 |
| iBOT | 0.72 | 0.70 | 0.74 | 0.72 | 0.72 | 0.72 |

5.6. On the Reward-aware Bisimulation Encoder

Prior work on bisimulation-based MPC incorporates an explicit reward predictor as part of the bisimulation objective to estimate rewards for planning (Shimizu & Tomizuka, 2025) (see Appendix A.1). While such a design is important for value approximation or policy transfer, it is not fundamental for our JEPA. Here the goal is to learn an invariant latent representation that preserves control-relevant transition dynamics rather than task-specific reward structure.

Empirically, when a reward predictor is included, Figure 11 shows that the reward distance converges to near zero early in training and provides little additional signal for improving accuracy in the transition dynamics. This suggests that, for the PointMaze task, reward prediction does not contribute beyond what is already captured by the transition dynamics.

6. Discussions and Future Work

We show that DINO-WM is not robust under background changes and distractors. By enforcing control-relevant invariance via bisimulation on top of pretrained visual features, we obtain latent embeddings $10\times$ lower-dimensional than that of DINO-WM that are robust for planning under visual

shifts, without reward supervision.

We note two key limitations of our work: 1) we assume access to sufficiently informative pretrained visual features. While we show robustness across different self-supervised encoders (Table 2), performance degrades when the visual representations lack semantic structure (i.e., without DI-NOv2), indicating that bisimulation-based invariance cannot compensate for poor visual features. 2) Our theoretical analysis focuses on reward-free bisimulation with goal-reaching costs and yields a horizon-dependent bound. While this aligns with JEPAs, it yields looser bounds than its reward-aware counterpart. Understanding whether $\mathcal{O}(T)$ is fundamental remains open.

Several directions come naturally from this work. First, we can integrate the bisimulation encoder in gradient-based planning (Parthasarathy et al., 2025), which may benefit from smoother and invariant latent dynamics. Another direction is to combine the bisimulation invariance with adaptive policies, enabling online refinement of the invariant representation as the agent encounters new visual conditions.

From a theoretical perspective, extending our analysis to reward-aware bisimulation could clarify the trade-offs between JEPAs’ modularity and tighter generalization bounds. Finally, considering complex manipulation tasks and long-horizon planning problems is under current implementation.

Impact Statement

This work aims to advance robust, task-agnostic visual world models for planning by improving representation learning under visual distribution shifts. There are many potential societal impacts of this work, none of which we feel must be specifically highlighted here.

Acknowledgments

The authors thank Vlad Sobal and Tim G. J. Rudner for instructive discussions on this work. Leonardo F. Toso is funded by the Center for AI and Responsible Financial Innovation (CAIRFI) Fellowship and by the Columbia Presidential Fellowship. James Anderson is partially funded by NSF grants ECCS 2144634 and 2231350 and the Columbia Center of AI Technology in collaboration with Amazon.

References

- Abate, A. Approximation metrics based on probabilistic bisimulations for general state-space markov processes: a survey. *Electronic Notes in Theoretical Computer Science*, 297:3–25, 2013.
- Assran, M., Duval, Q., Misra, I., Bojanowski, P., Vincent, P., Rabbat, M., LeCun, Y., and Ballas, N. Self-supervised learning from images with a joint-embedding predictive architecture. In *Proceedings of the IEEE/CVF Conference on Computer Vision and Pattern Recognition*, pp. 15619–15629, 2023.
- Balestriero, R. and LeCun, Y. Lejepa: Provable and scalable self-supervised learning without the heuristics. *arXiv preprint arXiv:2511.08544*, 2025.
- Bardes, A., Ponce, J., and LeCun, Y. Vicreg: Variance-invariance-covariance regularization for self-supervised learning. *arXiv preprint arXiv:2105.04906*, 2021.
- Caron, M., Touvron, H., Misra, I., Jégou, H., Mairal, J., Bojanowski, P., and Joulin, A. Emerging properties in self-supervised vision transformers. In *Proceedings of the IEEE/CVF international conference on computer vision*, pp. 9650–9660, 2021.
- Castro, P. and Precup, D. Using bisimulation for policy transfer in mdps. In *Proceedings of the AAAI conference on artificial intelligence*, volume 24, pp. 1065–1070, 2010.
- Castro, P. S. Scalable methods for computing state similarity in deterministic markov decision processes. In *Proceedings of the AAAI Conference on Artificial Intelligence*, volume 34, pp. 10069–10076, 2020.
- Castro, P. S., Panangaden, P., and Precup, D. Equivalence relations in fully and partially observable markov decision processes. In *IJCAI*, volume 9, pp. 1653–1658, 2009.
- Dosovitskiy, A. An image is worth 16x16 words: Transformers for image recognition at scale. *arXiv preprint arXiv:2010.11929*, 2020.
- Ebert, F., Finn, C., Dasari, S., Xie, A., Lee, A., and Levine, S. Visual foresight: Model-based deep reinforcement learning for vision-based robotic control. *arXiv preprint arXiv:1812.00568*, 2018.
- Ferns, N., Panangaden, P., and Precup, D. Metrics for finite markov decision processes. In *UAI*, volume 4, pp. 162–169, 2004.
- Ferns, N., Panangaden, P., and Precup, D. Bisimulation metrics for continuous markov decision processes. *SIAM Journal on Computing*, 40(6):1662–1714, 2011.
- Fu, J., Kumar, A., Nachum, O., Tucker, G., and Levine, S. D4rl: Datasets for deep data-driven reinforcement learning. *arXiv preprint arXiv:2004.07219*, 2020.
- Givens, C. R. and Shortt, R. M. A class of wasserstein metrics for probability distributions. *Michigan Mathematical Journal*, 31(2):231–240, 1984.
- Grill, J.-B., Strub, F., Altché, F., Tallec, C., Richemond, P., Buchatskaya, E., Doersch, C., Avila Pires, B., Guo, Z., Gheshlaghi Azar, M., et al. Bootstrap your own latent: a new approach to self-supervised learning. *Advances in*

- neural information processing systems*, 33:21271–21284, 2020.
- Ha, D. and Schmidhuber, J. World models. *arXiv preprint arXiv:1803.10122*, 2(3), 2018.
- Hafner, D., Lillicrap, T., Fischer, I., Villegas, R., Ha, D., Lee, H., and Davidson, J. Learning latent dynamics for planning from pixels. In *International conference on machine learning*, pp. 2555–2565. PMLR, 2019.
- Hafner, D., Lillicrap, T., Ba, J., and Norouzi, M. Dream to control: Learning behaviors by latent imagination. In *International Conference on Learning Representations*, 2020.
- Hafner, D., Lillicrap, T. P., Norouzi, M., and Ba, J. Mastering atari with discrete world models. In *International Conference on Learning Representations*, 2021.
- He, K., Chen, X., Xie, S., Li, Y., Dollár, P., and Girshick, R. Masked autoencoders are scalable vision learners. In *Proceedings of the IEEE/CVF conference on computer vision and pattern recognition*, pp. 16000–16009, 2022.
- Jiang, D., Liu, Y., Liu, S., Zhao, J., Zhang, H., Gao, Z., Zhang, X., Li, J., and Xiong, H. From clip to dino: Visual encoders shout in multi-modal large language models. *arXiv preprint arXiv:2310.08825*, 2023.
- Kemertas, M. and Aumentado-Armstrong, T. Towards robust bisimulation metric learning. *Advances in Neural Information Processing Systems*, 34:4764–4777, 2021.
- Khorrambakht, R., Ortiz-Haro, J., Amigo, J., Mostafa, O., Dugas, D., Meier, F., and Righetti, L. Worldplanner: Monte carlo tree search and mpc with action-conditioned visual world models. *arXiv preprint arXiv:2511.03077*, 2025.
- Kouvaritakis, B. and Cannon, M. Model predictive control. *Switzerland: Springer International Publishing*, 38(13-56):7, 2016.
- LeCun, Y. A path towards autonomous machine intelligence version 0.9. 2, 2022-06-27. *Open Review*, 62(1):1–62, 2022.
- Lenz, I., Knepper, R. A., and Saxena, A. Deepmpc: Learning deep latent features for model predictive control. In *Robotics: Science and Systems*, volume 10, pp. 25. Rome, Italy, 2015.
- Matsuo, Y., LeCun, Y., Sahani, M., Precup, D., Silver, D., Sugiyama, M., Uchibe, E., and Morimoto, J. Deep learning, reinforcement learning, and world models. *Neural Networks*, 152:267–275, 2022.
- Oquab, M., Darcet, T., Moutakanni, T., Vo, H., Szafraniec, M., Khalidov, V., Fernandez, P., Haziza, D., Massa, F., El-Nouby, A., et al. Dinov2: Learning robust visual features without supervision. *arXiv preprint arXiv:2304.07193*, 2023.
- Parthasarathy, A., Kalra, N., Agrawal, R., LeCun, Y., Bounou, O., Izmailov, P., and Goldblum, M. Closing the train-test gap in world models for gradient-based planning. *arXiv preprint arXiv:2512.09929*, 2025.
- Rubinstein, R. Y. and Kroese, D. P. *The cross-entropy method: a unified approach to combinatorial optimization, Monte-Carlo simulation and machine learning*. Springer Science & Business Media, 2004.
- Shadmehr, R. and Mussa-Ivaldi, S. *Biological Learning and Control: How the Brain Builds Representations, Predicts Events, and Makes Decisions*. The MIT Press, 2012.
- Shimizu, Y. and Tomizuka, M. Bisimulation metric for model predictive control. In *International Conference on Learning Representations*, 2025.
- Sobal, V., SV, J., Jalagam, S., Carion, N., Cho, K., and LeCun, Y. Joint embedding predictive architectures focus on slow features. *arXiv preprint arXiv:2211.10831*, 2022.
- Sobal, V., Zhang, W., Cho, K., Balestriero, R., Rudner, T. G., and LeCun, Y. Learning from reward-free offline data: A case for planning with latent dynamics models. *arXiv preprint arXiv:2502.14819*, 2025.
- Thuruthel, T. G., Falotico, E., Renda, F., and Laschi, C. Model-based reinforcement learning for closed-loop dynamic control of soft robotic manipulators. *IEEE Transactions on Robotics*, 35(1):124–134, 2018.
- Tkachev, I. and Abate, A. On infinite-horizon probabilistic properties and stochastic bisimulation functions. In *2011 50th IEEE Conference on Decision and Control and European Control Conference*, pp. 526–531. IEEE, 2011.
- Tobin, J., Fong, R., Ray, A., Schneider, J., Zaremba, W., and Abbeel, P. Domain randomization for transferring deep neural networks from simulation to the real world. In *2017 IEEE/RSJ international conference on intelligent robots and systems (IROS)*, pp. 23–30. IEEE, 2017.
- Villani, C. et al. *Optimal transport: old and new*, volume 338. Springer, 2008.
- Williams, G., Wagener, N., Goldfain, B., Drews, P., Rehg, J. M., Boots, B., and Theodorou, E. A. Information theoretic mpc for model-based reinforcement learning. In *2017 IEEE international conference on robotics and automation (ICRA)*, pp. 1714–1721. IEEE, 2017.

- Wu, Z., Zhang, J., Pai, D., Wang, X., Singh, C., Yang, J., Gao, J., and Ma, Y. Simplifying dino via coding rate regularization. *arXiv preprint arXiv:2502.10385*, 2025.
- Zhang, A., McAllister, R. T., Calandra, R., Gal, Y., and Levine, S. Learning invariant representations for reinforcement learning without reconstruction. In *International Conference on Learning Representations*, 2021.
- Zhou, G., Pan, H., LeCun, Y., and Pinto, L. DINO-WM: World models on pre-trained visual features enable zero-shot planning. In *International Conference on Machine Learning*, 2025.
- Zhou, J., Wei, C., Wang, H., Shen, W., Xie, C., Yuille, A., and Kong, T. ibot: Image bert pre-training with online tokenizer. *arXiv preprint arXiv:2111.07832*, 2021.
- Zhu, J., Evtimova, K., Chen, Y., Shwartz-Ziv, R., and LeCun, Y. Variance-covariance regularization improves representation learning. *arXiv preprint arXiv:2306.13292*, 2023.

A. Appendix

This appendix provides additional details that complement the main text. We include specifics on the architecture and implementation of the proposed bisimulation encoder and transition model, further discussion of the PCA-based variance-covariance regularization, and extended descriptions of the experimental setup, including task configurations, domain randomization, and planning details. We also provide the proofs for the generalization bound in Section 4.6.

A.1. Model Architecture

This section provides additional details on the architecture of the proposed joint-embedding predictive world model with bisimulation encoder.

A.1.1. OVERVIEW

The DINO-Bisim model takes visual observations, proprioceptive inputs, and actions at the current timestep and predicts the next bisimulation latent state, along with an optional reward prediction. Visual observations are encoded using a pretrained DINOv2 ViT-S/14 visual encoder (Oquab et al., 2023), followed by a bisimulation encoder implemented as an MLP to produce the latent state. Proprioceptive inputs and actions are embedded using lightweight 1D convolutional encoders. The resulting embeddings are concatenated and processed by a 6-layer transformer to predict the next bisimulation latent state. A separate reward MLP predicts the reward from the latent state, however, this component is not used in our experiments, as discussed in Section 5 and throughout the main text.

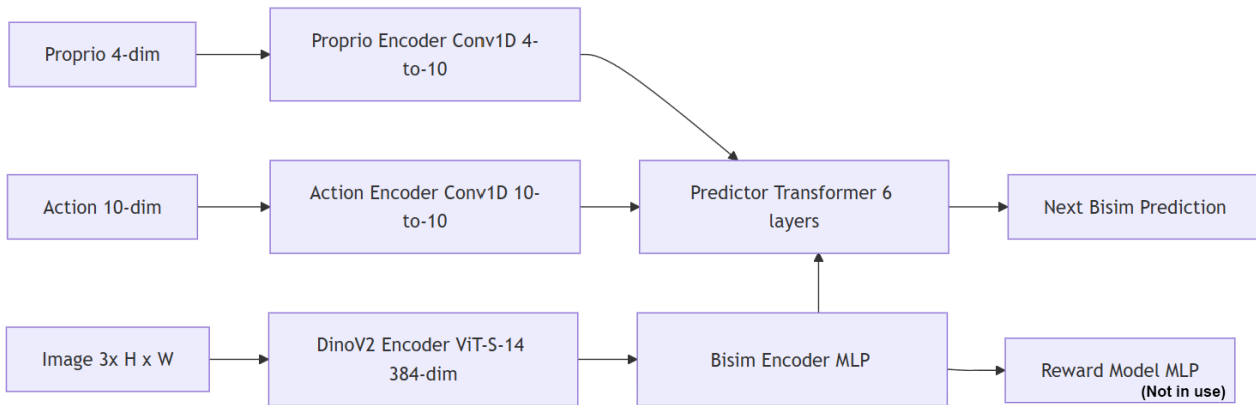


Figure 5. Overview of the DINO-Bisim architecture.

A.1.2. BISIMULATION MEMORY BUFFER (REPLAY BUFFER)

Recalling the definition of the bisimulation metric introduced in Section 3.2 and in (Castro, 2020), the corresponding loss involves computing differences between selected pairs of states. Since a single training iteration can only leverage the current batch of 20 states, we introduce a bisimulation memory buffer that stores up to 1000 previously generated states, also following (Zhang et al., 2021). This buffer allows comparisons with a larger and more diverse set of past states, thereby improving the stability and effectiveness of the bisimulation representation learning.

A.1.3. PATCH DESIGN IN BISIMULATION MODEL

Why Patch-based Design? The bisimulation model adopts a patch-based design, in which visual inputs are partitioned into spatial patches and each patch is encoded independently. This design builds upon the bisimulation encoder in (Shimizu & Tomizuka, 2025) and naturally aligns with the output format of DINOv2 and other patch-based visual encoders. Beyond architectural compatibility, the patch-based formulation substantially reduces the number of trainable parameters, leading to a more compact and efficient model while empirically improving performance.

More concretely, an example architecture using the hyperparameters in Table 4 is illustrated in Figure 6. Rather than

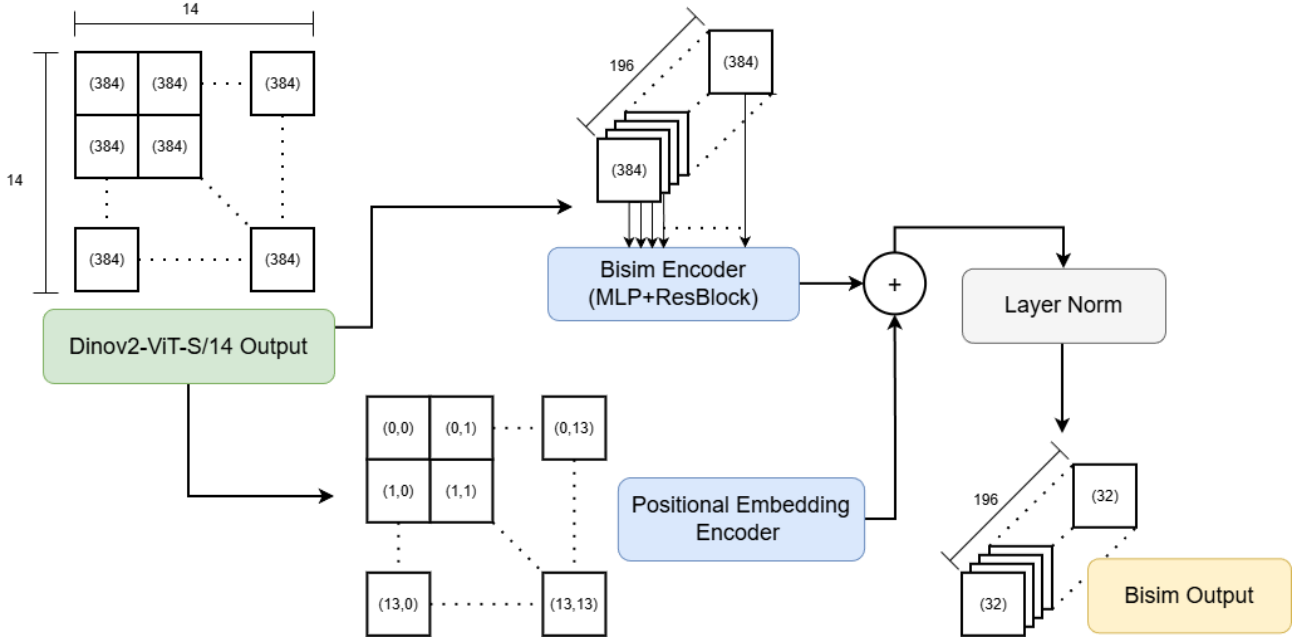


Figure 6. Bisimulation encoder with patch-based design, with 196 of patches and 32 output patch dimension.

flattening a feature map of size $14 \times 14 \times 384$ into a 75264-dimensional vector as input to the first layer, the patch-based bisimulation encoder performs 196 parallel forward passes using a shared MLP whose input dimension is 384. As a result, the number of parameters in the first layer is reduced from $(75,264 \times 256) + 256 = 19,267,840$ to $(384 \times 256) + 256 = 98,560$, where 256 is the hidden layer dimension, with only negligible additional overhead from the spatial embedding parameters.

Latent Space Dimensionality Comparison. DINO-WM operates on patch-based visual representations produced by DINOv2, consisting of 196 patches with 384-dimensional embeddings each, resulting in a latent representation of size 196×384 . In contrast, our patch-based bisimulation encoder preserves the same spatial structure but maps each patch to a low-dimensional latent embedding. This yields a representation of size 196×32 . Consequently, our model operates in a latent space that is more than $10\times$ smaller than that of DINO-WM, while maintaining improved robustness to slow, task-irrelevant features.

A.1.4. HYPERPARAMETERS

We now summarize the hyperparameters used in our experiments.

Table 3. Shared hyperparameters for DINO-Bisim training.

| Name | Value |
|------------------------------|--------|
| Image size | 224 |
| Optimizer | AdamW |
| Decoder learning rate | $3e-4$ |
| Predictor learning rate | $1e-5$ |
| Action encoder learning rate | $1e-4$ |
| Bisimulation learning rate | $5e-7$ |
| Action embedding dim. | 10 |
| Proprio embedding dim. | 10 |
| Epochs | 50 |
| Batch size | 20 |

Table 4. Bisimulation encoder hyperparameters.

| Name | Value |
|------------------------------------|-------|
| Bisimulation memory buffer size | 1000 |
| Bisimulation state comparison size | 200 |
| Action dim. | 10 |
| Num patches | 196 |
| Latent dim. | 32 |
| Patch dim. | 32 |
| Patch embedding dim. | 384 |

We list below the main hyperparameters used by the bisimulation encoder and transition model. These parameters control

the dimensionality of the latent representation, the size of the comparison set used for bisimulation representation learning, and the dimensionality of visual and action embeddings.

Bisimulation Memory Buffer Size and Comparison Size. The capacity of the bisimulation memory buffer and the number of stored latent states used for pairwise comparisons when computing the bisimulation loss.

Action Dimension (`action_dim`). The dimensionality of the encoded action representation, used as input to the reward predictor that is not in use for our experiments.

Number of Patches (`num_patches`). The number of spatial patches output by the bisimulation encoder, matching the patch decomposition of the visual pretrained encoder.

Latent Dimension (`latent_dim`). The dimensionality of the bisimulation latent space for each patch.

Patch Dimension (`patch_dim`). The dimensionality of each patch embedding produced by the bisimulation encoder; in our implementation, this is set equal to `latent_dim`.

Patch Embedding Dimension (`patch_emb_dim`). The dimensionality of the input patch embeddings provided by the pretrained visual encoder, matching the output dimension of DINOv2.

A.2. PCA-based Variance Covariance Regularization

Setup. Our experiments use DINOv2, SimDINOv2 and iBOT as pretrained visual encoder, which encode background appearance along the dominant principal components (see Section 4.3). As noted in the DINOv2 paper (Oquab et al., 2023), background information can be attenuated by thresholding the first principal component. Consistent with this observation and our illustration in Figures 3 and 8, we make the preliminary assessment that task-irrelevant appearance factors predominantly align with the first principal component direction in the latent feature space.

Method. The bisimulation encoder is initialized with random parameters and is first trained using the standard VICReg objective for a small number of epochs to stabilize representation learning. We then perform a one-time principal component analysis to identify the dominant direction associated with task-irrelevant variation. After a number of warm-up epochs, we replace the standard VICReg loss with the proposed PCA-based VICReg objective, which helps to suppresses variance along the identified principal component directions.

An example training run with a vectorized bisimulation latent representation of dimension 196×32 (corresponding to the number of patches and per-patch latent dimensionality), where PCA-based VICReg is enabled after $k = 50$ epochs, is shown in Figure 7.

Result. While this staged regularization approach improves the stability of invariant representation learning, we hypothesize that a tighter integration of PCA-based regularization throughout training and planning, rather than a discrete loss swap, could further enhance invariance. Exploring such joint objectives is an interesting direction for future work.

A.3. Additional Information on the Navigation Task

This section provides additional details on the simple navigation task used in our experiments, complementing the high-level description in the main text.

PointMaze (Fu et al., 2020) is a force-actuated 2-DoF navigation environment in which a ball moves in the Cartesian $x-y$ plane with the objective of reaching a target location. The agent observes proprioceptive state information and evolves under continuous dynamics that capture velocity, acceleration, and inertia. For a fair comparison, we train all models on 2000 fully random trajectories, matching the data setup in (Zhou et al., 2025). See Figure 9 for a sequence of frames that illustrates the planning from an initial state to a goal state.

A.4. Planning

We optimize the action sequence using CEM. At each step, CEM samples multiple candidate action sequences, rolls them out using the learned model, selects the sequences with lowest cost (3), and updates the sampling distribution accordingly. The first action of the optimized sequence is played, and the process repeats with a receding horizon.

Although gradient-based planning methods have recently been proposed and validated in (Parthasarathy et al., 2025) for

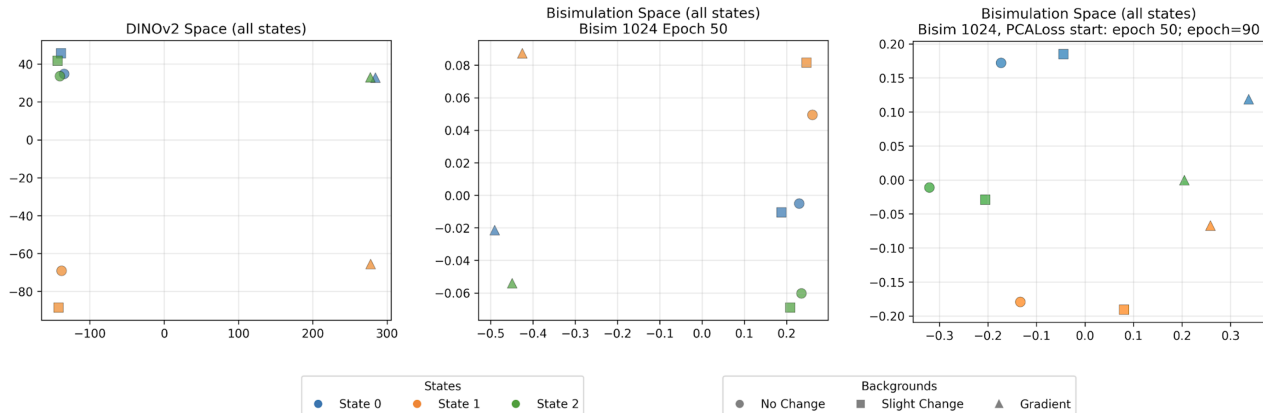


Figure 7. First two principal components (PCs) of three distinct states (colors) observed under three different backgrounds (marker shapes) for the PointMaze task. The goal of the bisimulation encoder is to map identical states across backgrounds to nearby latent representations. **Left.** DINOv2 embeddings $z_t = f_\theta(o_t)$ show strong separation along the first PC for identical states under different backgrounds, indicating that background variation dominates the leading principal direction. **Middle.** Bisimulation embeddings $w_t = h_\eta(z_t)$ after 50 epochs with standard VICReg still exhibit separation along the first PC, preserving background-dependent variation. **Right.** Bisimulation embeddings after 90 epochs with PCA-based VICReg (activated at epoch 50) show improved clustering of identical states across backgrounds, consistent with suppression of task-irrelevant variation.

DINO-WM, we focus on CEM for fair comparison with DINO-WM (Zhou et al., 2025).

A.5. Domain Randomization for the PointMaze Task

To evaluate robustness through data augmentation, we apply domain randomization to the PointMaze task by modifying the visual appearance of the environment during training. In particular, 40% of the training data are rendered with randomized visual backgrounds, while the remaining trajectories retain the default appearance. The randomization includes background color changes and gradient-based background modifications, as illustrated in Figure 10.

To avoid introducing spurious temporal artifacts that could make the transition dynamics learning harder, the randomized background is kept fixed within each trajectory but varies across different trajectories. Importantly, these visual modifications do not alter the underlying environment dynamics, agent behavior, or goal locations, ensuring that domain randomization affects only task-irrelevant visual features.

A.6. Reward-aware Bisimulation Encoder: Training Metrics

Let us now analyze the training dynamics of the reward-aware bisimulation encoder to assess the contribution of the reward prediction term relative to the transition-based objectives. Following prior work on bisimulation-based MPC (Shimizu & Tomizuka, 2025), we include an auxiliary reward predictor during training, although it is not used for training nor planning in our experiments.

Figure 11 reports the evolution of the main loss components throughout training. We observe that the reward prediction loss rapidly converges to near zero early in training and remains negligible afterwards. This indicates that, for the navigation task considered, reward prediction provides little additional learning signal beyond what is already captured by the transition dynamics. As a result, the reward term has a negligible influence on the learned latent representation.

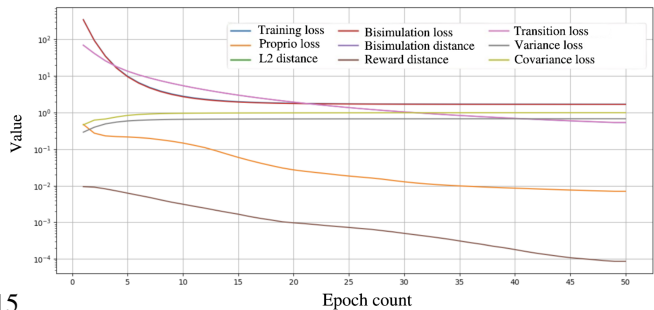


Figure 11. Training losses value versus the training epochs.

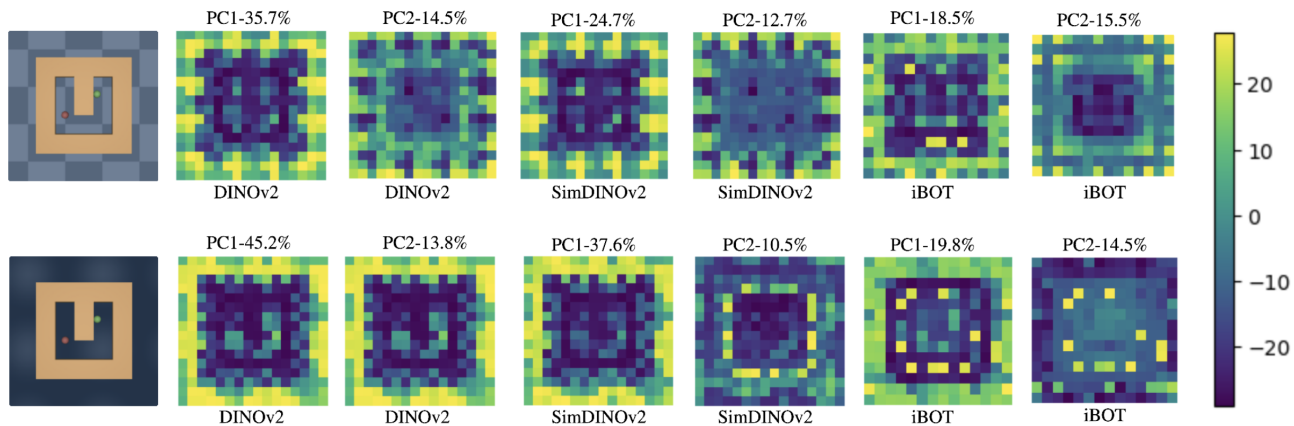


Figure 8. First two principal components (PC1 and PC2) of latent embeddings produced by DINOv2, SimDINOv2, and iBOT for a PointMaze observation. In all cases, PC1 captures a large percentage of the total variance that predominantly encodes background and layout information rather than control-relevant features.



Figure 9. PointMaze task, from leftmost the initial state to the rightmost the goal state

On the other hand, the transition losses and representation regularization terms (including the VICReg and bisimulation objectives) remain active throughout training and dominate the optimization process. These components are responsible for making the latent space to preserve control-relevant dynamics while suppressing task-irrelevant visual features. This empirical observation supports the design choice adopted in the main experiments, where we drop the reward prediction term and rely only on transition-based bisimulation to enforce invariance.

A.7. Moving Distractors

To evaluate robustness to dynamic but task-irrelevant visual variations, we consider two moving distractors in the PointMaze task. As illustrated in Figure 10, we augment the environment with colored distractor objects (yellow and magenta dots) that move continuously within the maze while remaining decoupled from the agent dynamics and task objectives.

The distractors introduce persistent motion that can dominate DINO-WM latent dynamics, despite being irrelevant for control. On the other hand our bisimulation-based representation is designed to suppress such task-irrelevant motion by enforcing equivalence between states that exhibit identical on-policy transition behavior. As a result, planning performance remains stable in the presence of moving distractors, whereas DINO-WM tend to drop in performance.

A.8. Reward-Free Generalization Bound: Proof of Theorem 4.1

We first provide an auxiliary lemma regarding the 1-Wasserstein distance which we use in the proof of Theorem 4.1.

Lemma A.1 (Kantorovich-Rubinstein duality (Villani et al., 2008)). *Let μ , and ν be two probability measures on the metric space (Ω, d_π) , then*

$$W_1(\mu, \nu) = \sup_{\|f\|_L \leq 1} (\mathbb{E}_{x \sim \mu}[f(x)] - \mathbb{E}_{y \sim \nu}[f(y)]), \quad (4)$$



Figure 10. Examples of domain-randomized visual observations for the PointMaze task. During training, background appearance is randomized across trajectories using color shifts, gradient backgrounds, and fixed distractors (i.e., the dot outside the maze) while the underlying maze layout and transition dynamics remain unchanged.

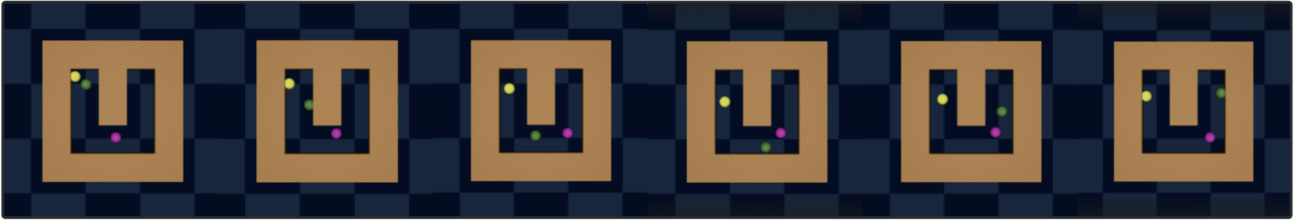


Figure 12. Moving distractor setting in PointMaze. Yellow and magenta dots move continuously within the maze, introducing dynamic but task-irrelevant visual variation while preserving the underlying transition dynamics.

where $\|\cdot\|_L$ is the Lipschitz norm (i.e., $\|f\|_L \leq \sup_{x \neq y} \frac{|f(x) - f(y)|}{|x - y|}$).

We will later invoke the auxiliary result above in the proofs of Theorem 4.1. To make this step explicit, we first show how the Kantorovich-Rubinstein duality implies a Lipschitz-based bound on differences of expectations. Let $\mu \triangleq P_\pi(\cdot | z)$, and $\nu \triangleq P_\pi(\cdot | z')$, be two probability measures on the metric space (Ω, d_π) , and define a scalar-valued function $s(\tilde{z})$ on the latent space z . Assuming that $s(z)$ is a L -Lipschitz with respect to d_π , i.e.,

$$|s(u) - s(v)| \leq L d_\pi(u, v), \quad \forall u, v \in \Omega.$$

By Kantorovich-Rubinstein duality (Lemma A.1), we have

$$W_1(\mu, \nu) = \sup_{\|f\|_L \leq 1} (\mathbb{E}_{x \sim \mu}[f(x)] - \mathbb{E}_{y \sim \nu}[f(y)]),$$

where $\|f\|_L \leq 1$ denotes that f is 1-Lipschitz with respect to d_π . Now define the rescaled function $l(\cdot) \triangleq \frac{1}{L} s(\cdot)$. Then l is 1-Lipschitz since, for all $u, v \in \Omega$, we have

$$|l(u) - l(v)| = \frac{1}{L} |s(u) - s(v)| \leq \frac{1}{L} L d_\pi(u, v) = d_\pi(u, v).$$

Thus l is feasible for the supremum in (4), implying that

$$W_1(\mu, \nu) \geq \mathbb{E}_{x \sim \mu}[l(x)] - \mathbb{E}_{y \sim \nu}[l(y)] = \frac{1}{L} (\mathbb{E}_{x \sim \mu}[s(x)] - \mathbb{E}_{y \sim \nu}[s(y)]).$$

Rearranging the terms, we obtain

$$\mathbb{E}_{x \sim \mu}[s(x)] - \mathbb{E}_{y \sim \nu}[s(y)] \leq LW_1(\mu, \nu). \quad (5)$$

Proof of Theorem 4.1: We begin the proof by first noticing that the goal-reaching cost used for planning is Lipschitz on the bounded set of bisimulation latent states, i.e., $\{w : \|w\|_2 \leq H_w\}$. Indeed, for any w, w' with $\|w\|_2, \|w'\|_2, \|w_g\|_2 \leq H_w$, we have the following expression

$$\begin{aligned} |c(w) - c(w')| &= \left| \|w - w_g\|_2^2 - \|w' - w_g\|_2^2 \right| \\ &= |\langle w - w', w + w' - 2w_g \rangle| \\ &\leq \|w - w'\|_2 \|w + w' - 2w_g\|_2 \quad (\text{Cauchy-Schwarz inequality}) \\ &\leq 4H_w \|w - w'\|_2, \end{aligned} \quad (6)$$

so $c(w)$ is $4H_w$ -Lipschitz.

We further write the recursion

$$J_T^\pi(z) = c(h_\eta(z)) + \gamma \mathbb{E}_{\tilde{z} \sim P_\pi(\cdot | z)} [J_{T-1}^\pi(\tilde{z})], \quad (7)$$

where we assume that $J_0^\pi(z) \equiv 0$.

We then prove by induction that J_T^π is L_T -Lipschitz with respect to $d_\pi(z, z')$, with $L_T \triangleq 8H_w T$, which implies (??).

For $T = 0$ it holds trivially. Assume it holds for $T - 1$. Then for any z, z' ,

$$|J_T^\pi(z) - J_T^\pi(z')| \leq |c(h_\eta(z)) - c(h_\eta(z'))| + \gamma \left| \mathbb{E}_{\tilde{z} \sim P_\pi(\cdot | z)} J_{T-1}^\pi(\tilde{z}) - \mathbb{E}_{\tilde{z}' \sim P_\pi(\cdot | z')} J_{T-1}^\pi(\tilde{z}') \right|.$$

Note that the first term is bounded by the quantity $4H_w \|h_\eta(z) - h_\eta(z')\|_2$. On the other hand, for the second term, since J_{T-1}^π is L_{T-1} -Lipschitz with respect to $d_\pi(z, z')$, we can use Kantorovich-Rubinstein duality to bound $\left| \mathbb{E}_{\tilde{z} \sim P_\pi(\cdot | z)} J_{T-1}^\pi(\tilde{z}) - \mathbb{E}_{\tilde{z}' \sim P_\pi(\cdot | z')} J_{T-1}^\pi(\tilde{z}') \right|$ by $L_{T-1} W_1(P_\pi(\cdot | z), P_\pi(\cdot | z'))$, i.e., by using (5).

Using the definition of the bisimulation metric, with the reward term dropped, we have $W_1(P_\pi(\cdot | z), P_\pi(\cdot | z')) = \gamma^{-1} d_\pi(z, z')$. Therefore, we obtain

$$|J_T^\pi(z) - J_T^\pi(z')| \leq 4H_w \|h_\eta(z) - h_\eta(z')\|_2 + L_{T-1} d_\pi(z, z').$$

As we assume that $\|h_\eta(z) - h_\eta(z')\|_2 \leq d_\pi(z, z') + \varepsilon$, then

$$|J_T^\pi(z) - J_T^\pi(z')| \leq (4H_w + L_{T-1}) d_\pi(z, z') + 4H_w \varepsilon. \quad (8)$$

Unrolling the recursion and assuming that ε is sufficiently small, i.e., $\varepsilon \leq d_\pi(z, z')$, then $L_T \triangleq 8H_w T$, which implies the bound as stated in Theorem 4.1.